PLACE + SPHERE: A Robust Approach for Correction of Susceptibility Artifacts in EPI

U. Techavipoo[1], S. Lai[1], I. Dimitrov[2], J. Lackey[1], J. Shi[1], and X. Guan[3,4]

[1]Radiology, Thomas Jefferson University, Philadelphia, PA, United States, [2]Philips Medical Systems, Best, Netherlands, [3]Computer Science, Stony Brook University, Stony Brook, NY, United States, [4]Neurosurgery, Thomas Jefferson University, Philadelphia, PA, United States

Introduction: Echo Planar Imaging (EPI) is commonly used in many imaging techniques such as diffusion tensor imaging (DTI) and functional MRI (fMRI) because of its fast acquisition. However, it suffers from the magnetic-field-inhomogeneity-induced geometric distortion at boundaries of tissues of different magnetic susceptibility such as air/tissue interfaces. The extent of this distortion depends on the amount of the susceptibility differences (which increases with the scanner magnetic field strength) and the total acquisition time for the k-space data. The longer the k-space data acquisition, the larger the phase aberration contained in the images. Quite a few distortion correction algorithms have been published, however, most them either are impractical because of their lengthy acquisition time or lack of stability. Most EPI images were therefore left distorted as they were obtained from the scanners. In general, the distortion correction algorithms were composed of two steps, i.e. mapping the field inhomogeneity and applying the maps to correct the distorted images. We are interested in the field mapping algorithm using the phase labeling for additional coordinate encoding (PLACE) [1] because of its short acquisition time and reliable results and the distortion correction algorithm using the simulated phase evolution rewinding (SPHERE) [2] because of its stability and simultaneous correction of the geometric and intensity distortions [3]. PLACE acquires at least two phase images to generate a field map. Instead of varying the echo time (TE) of each image as in many algorithms, it acquires data using almost the same sequence except for adding/removing an area equal to a multiple of a blip area to/from the pre-phase pulse in the phase encoding direction. This manipulation shifts a multiple of lines of the k-space data down/up from the original k-space data. The field maps from PLACE possess the same distorted spatial domain as the distorted images and easily pass to the SPHERE algorithm. SPHERE simulates the k-space data by re-phase-encoding each spatial location of a distorted image with additional inverse local phase errors generated from a given field map. After that, the simulated k-space data was inverse Fourier transformed to recover the original image. In this work, we developed a scheme that integrated the salient features of the PLACE and SPHERE algorithms, and developed a framework for examining the results with and without correction in terms of the normalized mutual information (NMI). The algorithm was also applied to correct susceptibility-induced distortion in DTI.

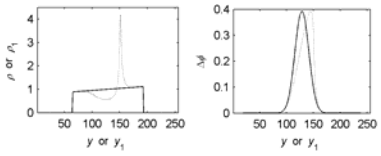

(a) (b)

FIG. 1: Simulation results of (a) the original (solid) and distorted (dotted) signals and (b) phase-shift maps on the original (solid) and distorted (dotted) spatial domains.

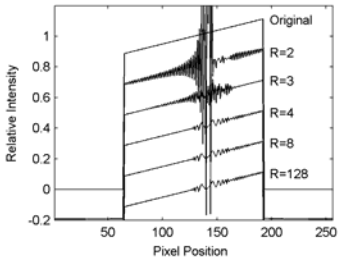

FIG. 2: Comparison of the recovered signals from the simulations using different sampling rates from 2 to 128.

Materials and Methods: The method to upsample the distorted images before applying SPHERE was investigated to obtain a suitable upsampling rate [3]. This was done by simulating a one-dimensional phantom signal with a known field map. After applying SPHERE, high frequency k-space components that extended from upsampling were removed before inverse Fourier transformation to recover the original image. All data were acquired on a 3T MR scanner (Achieva, Philips Medical System, Best, The Netherlands). A pulse sequence for field map acquisitions was created by modifying the DTI pulse sequence in order to duplicate its exact EPI trajectory and timing. First order flow compensation was applied to the slice-select direction to suppress the phase error caused by spins moving across the slices. For each slice, one T1-weighted image (T1WI) was acquired without pre-phase-pulse modification and four images were acquired with adding/removal of one or two blip areas from the pre-phase pulse, generating four field maps. The total acquisition time for this step was around 2 minutes (for five 60-slice T1WI volumes). The average field maps were then upsampled and applied directly to the SPHERE algorithm to correct the distortion in DTI data. We acquired four data sets of field maps, DTI data, and reference anatomical T1-weighted images (T1WIs) from four normal subjects. The DTI parameters were set to 32 diffusion-weighted directions, 256 to 300-mm FOV, 100% RFOV, 128 matrix size and reconstruction size, 2.5 to 3 SENSE reduction, single-shot EPI with shortest TE (around 80 ms) for a b-value of 850 s/mm^{-2}, 90° flip angle, shortest TR (around 8000 ms), for 60 slices of 2-mm thickness to cover the whole brain, Number of Signal Average equal to 3 for T2WIs and 1 for diffusion-weighted images. A 60-mm saturation band was applied inferior to the data volume to suppress phase interference from inflowing spins. Total DTI acquisition time was around 5 minutes. All computation was done using the MATLAB programming language version 7 (MathWorks, Inc., Natick, MA) on a PC with a 3.4-GHz CPU (Pentium 4, Intel Corporation, Santa Clara, CA) and 3.5-GByte RAM.

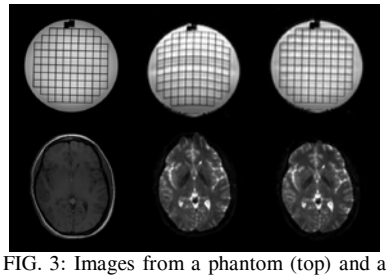

FIG. 3: Images from a phantom (top) and a brain (bottom) presenting T1WIs, distorted T2WIs, and recovered T2WIs (from 1st to 3rd columns) using the proposed algorithm.

Results: Figure 1 demonstrates the simulated one-dimensional signals, (a) the original (solid line) and distorted (dotted line) signals and (b) the field maps in terms of the phase shift according to the acquisition time from a k-space line to the next adjacent line. Figure 2 shows corrected one-dimensional images using upsampling ratio R = 2 to 128. As shown, no further improvement was seen for R > 4. Figure 3 illustrates phantom images (top row) and brain images (bottom row), where the first to the third columns present T1WIs, distorted T2WIs, and corrected T2WIs using the proposed algorithm. For the phantom images, the distorted geometry and intensity were restored except for the blurring that occurred in the upper half of the phantom. For the brain images, the elongated frontal lobe was restored to resemble the anatomical T1WI. The NMI values between the T1WI and the T2WIs before and after correction for this particular slice were improved from 1.0549 to 1.0645. The improved NMI values averaged across four subjects slicewise corresponding to the same brain structures are plotted on Fig. 4, where the slice numbers were ordered from inferior to superior. We used three major landmarks (the chiasm, the anterior commissure, and the superior edge of the corpus callosum, located around slices 16, 28, and 41, respectively) to separate the brains into four regions. This plot clearly implies that the algorithm reliably improves the NMI where the distortion severely occurred around the air sinuses anterior to the slices in region 2 and some adjacent slices in regions 1 and 3. Color-coded FA maps before and after correction are shown in Fig. 5.

Discussion and Conclusions: We have shown that the integration of PLACE to acquire field maps, SPHERE to correct the distortion, and the upsampling method provides stable geometric and intensity correction of susceptibility artifacts with practical acquisition time. The EPI trajectory and timing of the field map acquisitions and of the images to be corrected have to be perfectly matched. The DTI data after correction using the proposed method were aligned to their corresponding anatomical images better than those without correction. However, the algorithm cannot restore the image if its distortion is beyond a certain limit or caused by signal dropout through slices. This proposed method can be applied to any other imaging models using EPI such as fMRI.

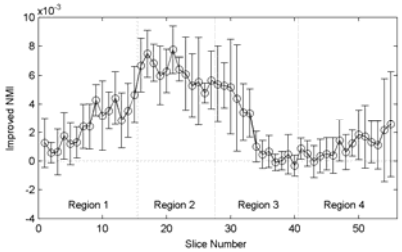

FIG. 4: A plot of improved NMI between T1WIs and T2WIs after correction averaged slicewise across 4 subjects. (±1 SD errorbar)

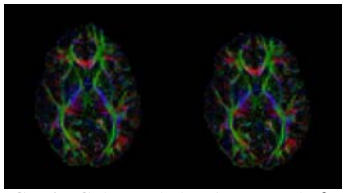

FIG. 5: Color-coded FA maps before (left) and after (right) correction.

References:

[1] Q. S. Xiang and F. Q. Ye, *ISMRM* 2006, pp. 2346.
[2] Y. M. Kadah and X. Hu, *MRM,* vol. 38, pp. 615-627, 1997.
[3] J. Y. Chiou, et al., *IEEE TMI,* vol. 22, pp. 200-205, 2003.